Received: 8 November 2017 | Revised: 28 April 2018 | Accepted: 29 May 2018 | Published on: 17 August 2018

DOI: 10.1002/joc.5740

International Journal of Climatology RMetS

RESEARCH ARTICLE

Low-level circulation and precipitation simulated by CMIP5 GCMS over southeastern South America

Vicente R. Barros | Moira E. Doyle

Centro de Investigaciones del Mar y la Atmósfera (CIMA, CONICET-UBA-UMIIFAECI), Departamento de Ciencias de la Atmósfera y los Océanos – Universidad de Buenos Aires, Buenos Aires, Argentina

Correspondence
Moira Doyle, Centro de Investigaciones del Mar y la Atmósfera (CIMA, CONICET-UBA-UMIIFAECI) Departamento de Ciencias de la Atmósfera y los Océanos – Universidad de Buenos Aires Ciudad Universitaria Pabellon II – 2do piso1428 Buenos Aires, Argentina.
Email: doyle@cima.fcen.uba.ar

Funding information
Consejo Nacional de Investigaciones Científicas y Técnicas, Grant/Award Number: PIP 11220120100586; Universidad de Buenos Aires, Grant/Award Number: UBACYT 20020130100644BA

Global climate models (GCMs) have, in general, problems representing precipitation over southern southeastern South America (SSESA), namely southern Brazil, Uruguay and eastern Argentina. In this study, 18 models were selected from the Coupled Model Inter-comparison Project Phase 5 to evaluate rainfall of the warm semester (October–March) when most of the rain takes place. Though GCMs reproduce the main features of the two main low-level circulation variability modes over southeastern South America, east of the Andes, particularly the two flow patterns associated with the active and weak SACZ, most of them underestimate the northern flow that brings water vapour into SSESA, as well as the mean precipitation in this region. According to an index that stands for the northern flow towards SSESA, all models, except one, have lower northern flow into SSESA than the observed reanalysis field. In addition, this index has a significant correlation across GCMs with mean SSESA precipitation, indicating that lower northern flow into SSESA is generally associated with a greater underestimation in the model precipitation. Hence, it is concluded that the weaker northern flow into SSESA simulated by most GCMs is a cause of their simulated lower precipitation in this region.

KEYWORDS
CMIP5, precipitation, principal component analysis, SESA, stream function

1 | INTRODUCTION

Understanding the water cycle and how it will be affected under increased greenhouse gas scenarios is of great importance to society and is subject of numerous studies worldwide. The Coupled Model Inter-comparison Projects, in their different phases, have made available numerous simulations for historical and future scenario conditions through which great advances in the understanding of this process have been obtained. The IPCC Fifth Assessment Report (AR5) (IPCC, 2013) however, states that, although large-scale patterns of precipitation have improved in the last generation simulations, models continue to perform less well for precipitation than for surface temperature. Studies by Stephens *et al*. (2010), Tian *et al*. (2013) and Demory *et al*. (2014) have concluded that global climate models (GCMs) in comparison to observations produce higher total precipitation amounts and a greater precipitation frequency which leads to a more active water cycle than the observed.

There are numerous studies evaluating CMIP3 and CMIP5 historical simulations of precipitation at global and local scales as well as the improvements obtained with the newer generation models. The evaluation of CMIP3 simulations showed that models are able to simulate large-scale mean climate conditions, such as the high rainfalls in the eastern and central tropical Pacific north of the equator, or areas with low precipitations like Northern Africa or eastern subtropical ocean basins (Dai, 2006). However, the representation of local features is quite limited (Boulanger *et al.,* 2007; Silvestri and Vera, 2008; Sakaguchi *et al.,* 2012; Gulizia *et al.,* 2013 among others). IPCC Fourth Assessment Report (AR4) (IPCC, 2007) noted that the difficulty in regional signals is due to the coarse model resolution and inadequate model physics. The increase in resolution in

some models (Delworth *et al.,* 2012) as well as better representations of sub-grid scale parameterizations of convection (Neale *et al.,* 2008), have shown substantial improvements in precipitation patterns. Consequently, simulations of mean precipitation in the CMIP5 ensemble present an overall improvement respect to the CMIP3 ensemble (Flato *et al.,* 2013).

Mehran *et al.* (2014) used several statistical measures to compare continental precipitation from 34 CMIP5 simulations against the Global Precipitation Climatology Project (GPCP) monthly mean observational estimates. They found that total monthly precipitation from most model simulations agree considerably well with observations, however deserts and sub-continental regions like central Australia and north-eastern Eurasia are problematical. They also identify overestimation of rainfall in regions with steep topography while on the lee side of the mountains the bias is negative. The tropical Atlantic has also been identified as region with precipitation biases in coupled and uncoupled GCMs. Some of these biases are overestimation of rainfall in the Caribbean and drier than normal conditions in Amazonia during the boreal summer (Davey *et al.,* 2002; Biasutti *et al.,* 2006; Stockdale *et al.,* 2006; Yin *et al.,* 2013). Other errors occurring in several models include an overly zonal orientation of the South-Pacific Convergence Zone (Brown *et al.,* 2013) as well as an overestimate of the frequency of occurrence of light rain events (Stephens *et al.,* 2010). Problems in the precipitation distribution have also been documented by several authors. Models tend to precipitate more frequently in light amounts (Dai, 2006; Sun *et al.,* 2007; Stephens *et al.,* 2010; Sillmann *et al.,* 2013) while there are few occasions when precipitation is caused by intense downbursts. These intense precipitations in extra-tropical regions are often caused by frontal systems (Catto *et al.,* 2012; Pfahl and Wernli, 2012), and though models are able to simulate the interaction of moisture and dynamics at grid scale (Catto *et al.,* 2010, 2013) they still underestimate precipitation events in frontal systems.

Several factors, such as moisture distribution over the continents, thermodynamics, and dynamical aspects, interact to determine the precipitation fields (Silva *et al.,* 2014). Modelling studies like the one presented by Schmittner *et al.* (2011) have demonstrated that alterations to global topography affect the climate system, in particular, modify moisture fluxes and ocean circulation (Levang and Schmitt, 2015). For example, the Andes mountains in models used in this study (Table 1) are represented with topography values between 2,653 (NorESM1-M) and 4,629 m (MIROC4h), while the highest peak actually reaches a height of 6,962 m. Richter and Xie (2010) showed that such underestimations may lead to excess moisture transport across mountains creating discrepancies in the precipitation fields. Besides the Andes there are other features in South America that are still not well represented in models which create rainfall biases.

In their analysis of historical CMIP5 simulations, Yin *et al.* (2013) show that some models still underestimate rainfall over Amazonia in different seasons. The biases found in precipitation are not the result of the misrepresentation of

TABLE 1 Description of 18 CMIP5 historical simulations used in the study. Period 1960–2012

GCM MODEL	Institution	Country	Resolution: (lon, lat, levels)	Highest topography in Southern South America (m)
CCSM4	National Center for Atmospheric Research	USA	288 × 200, L26	4,206
CMCC-CM	Centro Euro-Mediterraneo sui Cambiamenti Climatici	Italy	480 × 240, L31	4,568
CNRM-CM5	CNRM-GAME (Centre National de Recherches Meteorologiques—Groupe d'etudes de l'Atmosphere Meteorologique) and Cerfacs (Centre Europeen de Recherche et de Formation Avancee)	France	240 × 120, L31	4,388
CSIRO-Mk3-6	CSIRO Marine and Atmospheric Research and the Queensland Climate Change Centre of Excellence	Australia	192 × 96, L18	3,993
GFDL-ESM2M	Geophysical Fluid Dynamics Laboratory	USA	144 × 90, L24	3,489
HadCM3	UK Met Office Hadley Centre	UK	96 × 72, L19	3,843
HadGEM2-CC			192 × 144, L60	3,715
HadGEM2-ES			192 × 144, L38	3,715
INMCM4	Russian Institute for Numerical Mathematics	Russia	180 × 120, L21	3,588
IPSL-CM5A-LR	Institut Pierre Simon Laplace	France	96 × 95, L39	3,858
IPSL-CM5A-MR			144 × 143, L39	4,213
MIROC4h	University of Tokyo, National Institute for Environmental Studies, and Japan Agency for Marine-Earth Science and Technology	Japan	128 × 64, L80	4,629
MIROC5			128 × 64, L80	3,965
MIROC-ESM			640 × 320, L56	2,652
MPI-ESM-LR	Max Planck Institute for Meteorology	Germany	190 × 95, L47	4,147
MPI-ESM-MR			190 × 95, L95	4,147
MRI-CGCM3	Meteorological Research Institute	Japan	320 × 160, L48	4,303
NorESM1-M	Norwegian Climate Centre	Norway	144 × 96, L26	2,653

just one process. Most models underestimate convection and large-scale precipitation during the dry season, however in some models too much surface net radiation and a resultant high Bowen ratio seems to be the cause of negative biases. Models where moisture convergence and evapotranspiration are more realistic generally have more realistic rainfall totals in dry and transition periods. However, the authors conclude that, factors such as low pre-seasonal latent heat, high sensible flux, and a weaker influence of cold air incursions when 200 hPa zonal winds are excessively strong over the southern Amazon, contribute to the dry bias in transition seasons.

Precipitation in the historical model simulations has also been analysed in other areas of South America. Simulations tend to underestimate precipitation over Southeastern South America (SESA), the South Atlantic Convergence Zone (SACZ) (Vera *et al.,* 2006a; Gulizia and Camilloni, 2015) and more specifically over eastern Argentina (Vera *et al.,* 2006a, 2006b; Bombardi and Carvalho, 2011; Gulizia *et al.,* 2013). Though AR5 models have improved with respect to previous versions, this underestimation still persists (Blazquez and Nuñez, 2013; Jones and Carvalho, 2013; Gulizia and Camilloni, 2015) and the processes leading to this bias have not been clearly identified yet. Jones and Carvalho (2013) studied the representation of the South American Monsoon System (SAMS) and concluded that models coherently show positive increases in the amplitude, early onset, late demise, and duration of the SAMS during 1951–2005. In their analysis of the North American monsoon system Geil *et al.* (2013) examined 21 models and found an inaccurate representation of gradients in low-level geopotential height which causes an unrealistic low-level moisture topical flux affecting the retreat of the monsoon.

A dipole variability pattern (Nogués-Paegle and Mo, 1997), dominated by a strong SACZ at one phase and a weaker SACZ at the opposite phase modulates summer precipitation in SESA. This circulation is strongly dependent on atmospheric low-level moisture. Trade winds entering the continent from the tropical Atlantic provide moisture to the Amazon Basin (Zhou and Lau, 1998). After crossing the Amazon Basin, the low-level winds are blocked by the Andes Mountains and channelled southward into two possible circulations which characterize the dipole pattern. When the flow has a strong southward component, it establishes the South American Low-Level Jet, transporting large amounts of moisture to Paraguay, north and eastern Argentina, Uruguay and southern Brazil and consequently enhancing precipitation. In contrast, the SACZ region receives less amount of moisture weakening the precipitation regime. The second circulation observed as part of the dipole pattern is dominated by pronounced eastward component which transports moisture to the SACZ where rainfall is enhanced (Carvalho *et al.,* 2004). During the active SACZ, southern SESA (SSESA) is characterized by dry summer seasons as a result of the compensatory subsidence over the region (Gandú and Silva Días, 1998).

In average rainfall in SESA between October and March, from now on warm season, accounts for two thirds of the annual precipitation and has a double peak in late spring and late summer. However, the interannual variability of the dipole pattern associated with the SACZ (Doyle and Barros, 2002; Barros *et al.,* 2008) may modify the annual pattern (Grimm *et al.,* 2000; Penalba and Vargas, 2008; Solman *et al.,* 2008). Gulizia *et al.* (2013) analysed water vapour transport, convergence and precipitation in CMIP3 historical simulations and concluded that GCMs capture only some aspects of the observed patterns in southeastern South America, leaving the question of why precipitation is underestimated in SESA still unanswered.

In this study 18 CMIP5 models are analysed in an attempt to understand why models misrepresent warm season rainfall in SSESA. Considering the discussion presented on the different processes related to precipitation which models are still not able to solve adequately, and given that low level circulation driving moisture flux is a key factor to determine which phase of the oscillation will dominate in SESA, this process is evaluated in the historical model simulations to determine if its misrepresentation is one of the factors leading to precipitation underestimation.

The paper is structured as follows. Section 2 describes data sources and lists the GCMs analysed. As a necessary background, the observed low-level variability circulation of the warm season and its relation with the precipitation are reviewed in Sections 3 and 4, updating previous work (Barros *et al.,* 2008), until 2012. GCMs low level circulation variability is discussed in Section 5, while the relation between this low level circulation representation and precipitation underestimation is done in Section 6. Section 7 wraps up the main conclusions.

2 | DATA AND METHODOLOGY

Monthly precipitation series covering the period 1960–2012 were obtained from the Argentine National Weather Service, the Brazilian National Electric Energy Agency (ANEEL) and the Global Historical Climatology Network (GHCN), (Lawrimore *et al.,* 2011). Only those series with the smallest percentage of missing data (less than 10%) were retained. The selected 175 stations, Figure 1, are not homogenously distributed in space, thus, precipitation observations were re-projected to a $3^\circ \times 3^\circ$ mesh using the Kriging interpolation method (Cressie, 1991) to get results independent of the station density distribution. The analysis is restricted to austral warm season months (October–March) when the SACZ shows strongest activity and most of the precipitation is observed. Monthly zonal and meridional wind fields at 925 hPa are taken from National Center for Atmospheric Research–National Centers for Environmental Research

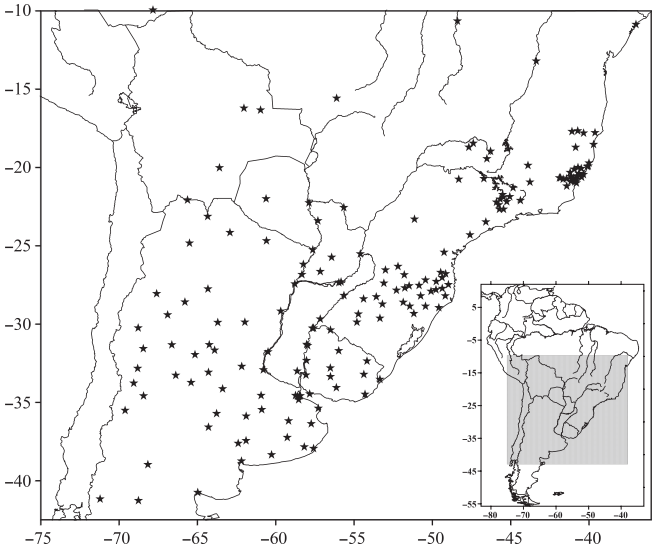

FIGURE 1 Precipitation stations included in the analysis

(NCEP–NCAR) reanalysis archive, with resolution of 2.5° latitude–longitude (Kalnay *et al.,* 1996; Kistler *et al.,* 2001).

The Coupled Model Intercomparison Project Phase 5 (CMIP5) coordinated major international research institutions and groups to conduct climate projection experiments using state-of-the-art models with higher resolution representing physical, chemical, hydrological, and oceanic processes, with a same set of prescribed greenhouse gases (GHG) emission scenarios (Taylor *et al.,* 2012). Monthly data of simulations from 18 GCM experiments were selected for the present study based on a previous study for the region (Gulizia and Camilloni, 2015). Table 1 shows a short description of the CMIP5 models analysed, indicating horizontal resolution (number of grid points over the global atmosphere), vertical levels, the maximum altitude and the institution where they were run. The analysed simulations include natural and anthropogenic forcing and are part of the *historical* experiment starting in 1850 and ending in 2005. The time period was extended from 2006 to 2012 to match the observation period, using wind data from the simulations representing the likely future change with RCP4.5 scenario. In this study, only *r1i1p1 runs* for each model were considered. Given the different horizontal resolution of the different models, *u* and *v* wind components were re-gridded to the NCEP Reanalysis grid (2.5° × 2.5°) applying linear interpolation.

To include moisture advection from the Atlantic Oceans and tropical South America, associated with the rainfall over the SESA, the area from 70°–20°W and 45°–10°S is considered in the low level atmospheric characteristic analysis. Circulation features are represented through the stream function derived applying psi function from GrADS fish library (Da Silva, 2007) to reanalysis and model wind data.

The main patterns of variability, in decreasing order of the associated variance, of the low level flow are identified performing a T mode principal component analysis (PCA) to the 925 hPa stream function field correlation matrix (Rencher, 1998). The first 6 PCAs, which in each case cumulatively explain more than 95% of the total variance in the stream function field, and met the Kaiser criterion (PCs with eigenvalues greater than 1) were rotated using orthogonal varimax. With this rotation method the spatial extent of regions with strong correlations is minimized, the PCs have more localized structures, and thus may be more amenable to physical interpretation (Richman, 1986).

The patterns of the two principal warm semester circulation modes obtained through PCA for reanalysis and models were evaluated through Taylor diagrams (Taylor, 2001). These diagrams graphically summarize the fit between models and observations quantified through three parameters: correlation, root mean square difference and the amplitude of the *SD*s. The performance of model precipitation with respect to observation during the warm semester is also evaluated through Taylor diagrams and estimating the relative error and coefficient of variation of the mean fields. The relative error was calculated considering the percentages of the warm season observed rainfall that are represented by each model and for each 3 × 3°grid point using the following expression:

$$\mathrm{RE} = \frac{\mathrm{Prec}_{\mathrm{mod}} - \mathrm{Prec}_{\mathrm{obs}}}{\mathrm{Prec}_{\mathrm{obs}}} * 100. \quad (1)$$

Finally, to estimate if the interannual variability of the warm semester precipitation in models is similar to the observed the coefficient of variation defined as

$$\mathrm{CV} = \frac{\mathrm{std}(\mathrm{prec}_{\mathrm{mod}}) \big/ \overline{\mathrm{prec}}_{\mathrm{mod}}}{\mathrm{std}(\mathrm{prec}_{\mathrm{obs}}) \big/ \overline{\mathrm{prec}}_{\mathrm{obs}}}, \quad (2)$$

is calculated allowing to detect a change in *SD* that is not simply related to a variation in mean precipitation.

3 | WARM SEASON LOW-LEVEL VARIABILITY CIRCULATION

The study of the low-level circulation variability was done on the October–March semester, when the precipitation dipole pattern is observed (Nogués-Paegle and Mo, 1997; Marengo *et al.,* 2012; Boers *et al.,* 2014). The domain for the analysis of the low-level flow includes the western part of the South Atlantic High over the nearby Atlantic Ocean and extends west up to 70°W, Figure 2. It captures the main moist flows over SESA that come from the ocean and from the tropical forests as discussed in Doyle and Barros (2002).

The first and second principal components (PC1 and PC2) explain 48.3 and 44.2% of the variance accounting together for more than 90% of the total variance. The next component, PC3 only explains 1.3%. Therefore the analysis can be focused on the first two modes, without losing significant information.

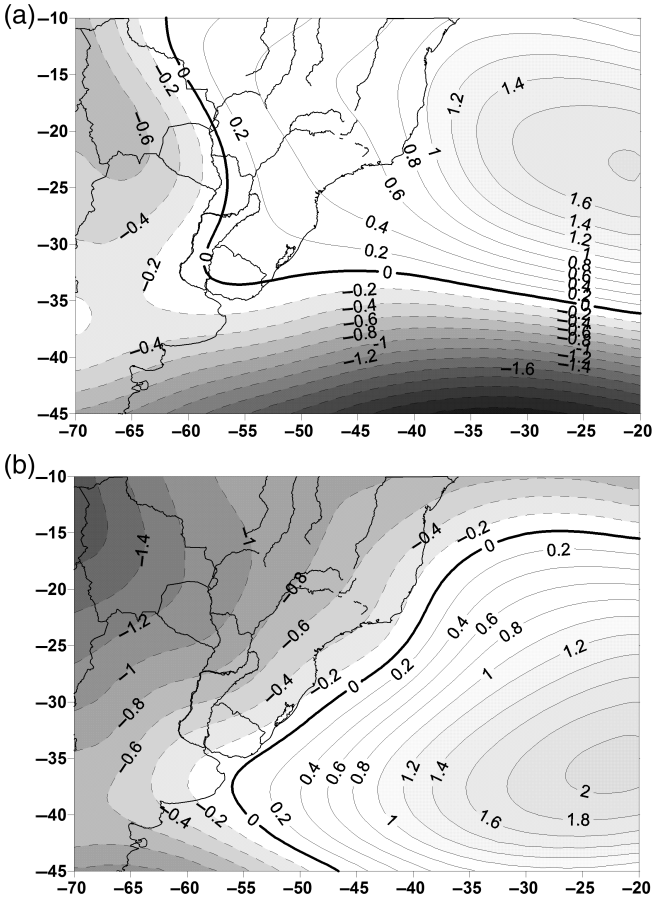

FIGURE 2 Rotated mode T principal components of the streamflow at 925 hPa for October–March period during 1960–2012. (a) PC1 and (b) PC2

The main atmospheric circulation features synthesized by the first two principal components are shown in Figure 2. Mode 1 depicts a pattern with a strong flow from the South American tropical forests over Eastern Argentina, Uruguay and southernmost Brazil until the Plata River mouth. The south Atlantic high pressure system is centred between 20° and 25°S highly influencing the circulation in the Brazilian coast. This pattern is representing the characteristic features of the circulation during the case of a weak SACZ (Doyle and Barros, 2002 their figure 15). Mode 2 shows a pronounced southward shift of the South Atlantic High circulation, which corresponds to the strong phase of the SACZ, although the eastward flow transporting moisture from the Amazon towards the SACZ is not represented because the domain chosen privileges the circulation over eastern Argentina. Though the branch from the west flow over the SACZ is lacking, however the descending compensatory movement can be inferred from the anticyclonic circulation to the south of this system. These two main 925 hPa stream flow patterns are consistent with the main features of the patterns obtained by Barros *et al*. (2008) when analysing precipitation trends in the region and their relation with sea level pressure variability.

The variability of these first two components with time is shown by the respective factor loadings, Figure 3a. The complementary variability between these factor loadings suggests that the circulation in the warm semester alternate between two main patterns; hence, this alternate dominance of the first and second factor loadings is taken as a second element to link the two first modes to the flows which give place to the dipole rainfall pattern between SESA and SACZ. More evidence leading to this affirmation will be shown in the Section 4.

Linear trends of factor loadings 1 and 2 were calculated, and though not highly statistically significant (15% level) they are consistent with circulation changes observed by other authors. The trend in the first factor loading between 1960 and 2012 indicates a decrease in the importance of the first mode, which is compensated by the increasing trend in the second factor loading, as well as in their squared values (representing the explained variance). Moreover, at the end of the 20th Century these modes changed their order of importance. Since the second mode represents the anticyclonic circulation centred at higher latitudes, this change is consistent with a southern shift of the western part of the South Atlantic High (Camilloni *et al.,* 2004; Barros *et al.,* 2008; Polvani *et al.,* 2011; Yongyun *et al.,* 2011), associated with the systematic southward expansion of the southern branch of the Hadley during summer and autumn (Hu and Fu, 2007). In Figure 3b the squared values of each factor loading are presented representing the explained variance time series of these two components. Though the two variables explain approximately the same variance, as discussed above, however the distribution of the variance with time changes as indicated by the linear trends of each of the squared FL, in a similar way to the change in FL. These trends in the two first factor loadings of the main 925 hPa streamflow modes are also consistent with the trends found by Barros *et al*. (2008) when they analysed the main sea level pressure modes during the warm semester.

4 | PRECIPITATION AND LOW LEVEL CIRCULATION VARIABILITY

Precipitation trends in southeastern South America have had a positive sign since the 1960s as documented by several authors (Liebmann *et al.,* 2004; Barros *et al.,* 2008; Seager *et al.,* 2010; Mo and Berbery, 2011). Barros et al. (2008) showed that this increase in precipitation is mainly accounted for by the increase of the warm season rainfall which in turn is related to the southward shift of the south Atlantic high. Following their methodology Figure 4a shows the interannual correlation pattern between the warm season precipitation at each grid point and the factor loading of the first mode of the 925 hPa streamflow for the period 1960–2012. Statistically significant positive correlations over eastern Paraguay and Argentina, extreme southern Brazil and Uruguay are indicative of favoured precipitation in this area during the warm semester when the first mode prevails over the second. This is consistent with the northwest-southeast low level flow associated with this mode, which transports water vapour from the tropical forest enhancing

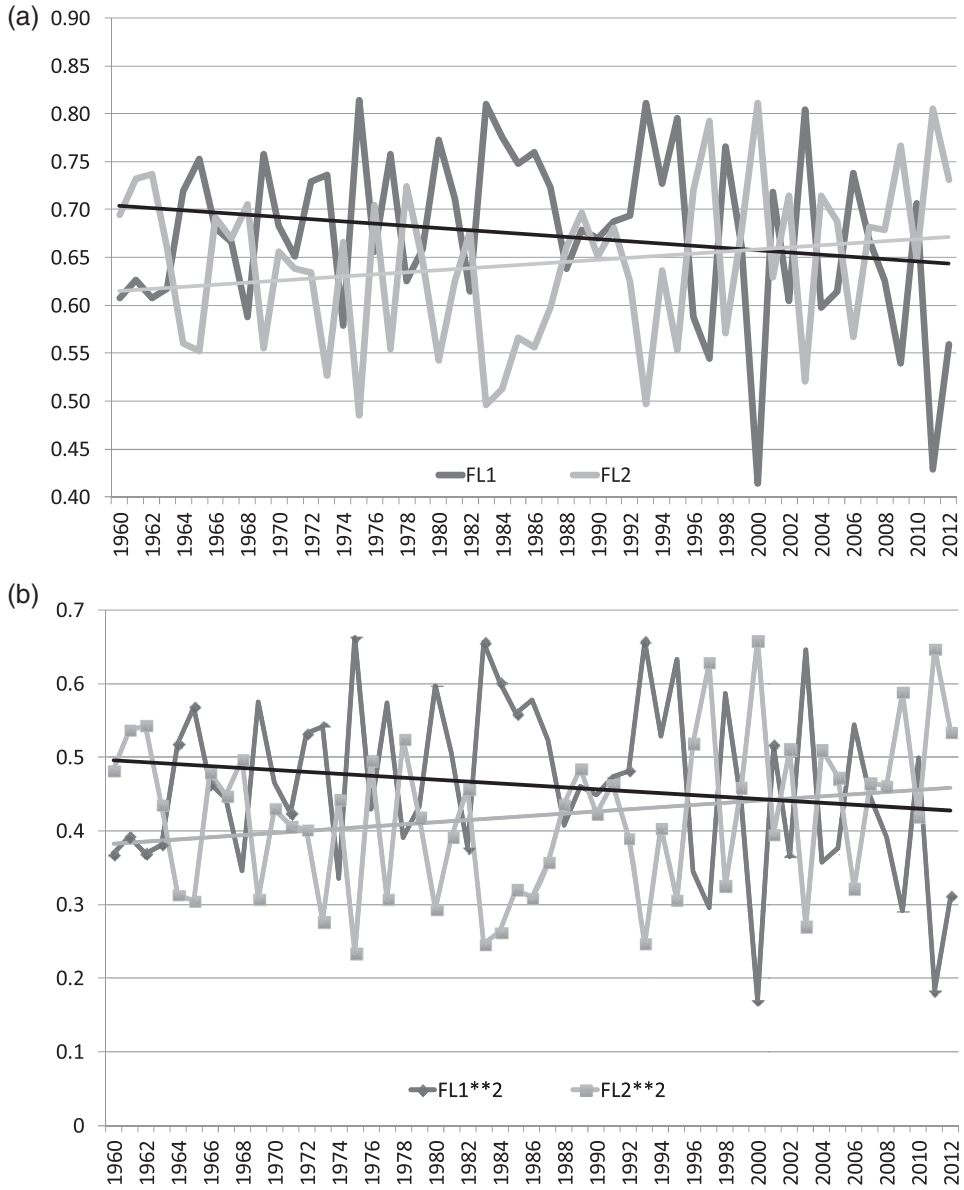

FIGURE 3 Warm season (a) factor loadings and (b) squared factor loadings indicative of the explained variance, for the first (black) and second (grey) modes and their linear trend

the likelihood of convective developments and rainfall. Hence, in this phase of the dipole the transport towards the continental SACZ from the tropical forest is not present inhibiting the possibility of precipitation, as represented by the negative correlations over the continental part of the SACZ.

To ensure that there is a true association between both variables (Kantelhardt *et al.,* 2001), the correlation was also calculated with the detrended series of both variables (Figure 4b). Nonetheless, in this last case the main features of the correlation pattern are conserved, indicating that in fact there is a real association between the low level Mode 1 and precipitation over SSESA.

In the case of Mode 2 (Figure 5a), the correlation pattern with precipitation is in general inverse to the one with Mode 1, with a negative correlation south of 23°S, significant at the core correlation area, and a positive correlation at the continental SACZ region, confirming the association of this mode with the active phase of the SACZ, which inhibits precipitation to the south of it with compensatory subsidence. Once again, the correlations of the detrended variables (Figure 5b) highlight the same areas of positive and negative association between rainfall and circulation, which dismisses a spurious correlation arising from the trends in both variables.

5 | GCMS MONTHLY VARIABILITY OF THE LOW LEVEL WARM SEASON CIRCULATION

We have seen that the two main modes of the low level circulation in the warm season are related to precipitation in the southern part of SESA. In addition, many GCMs fail to

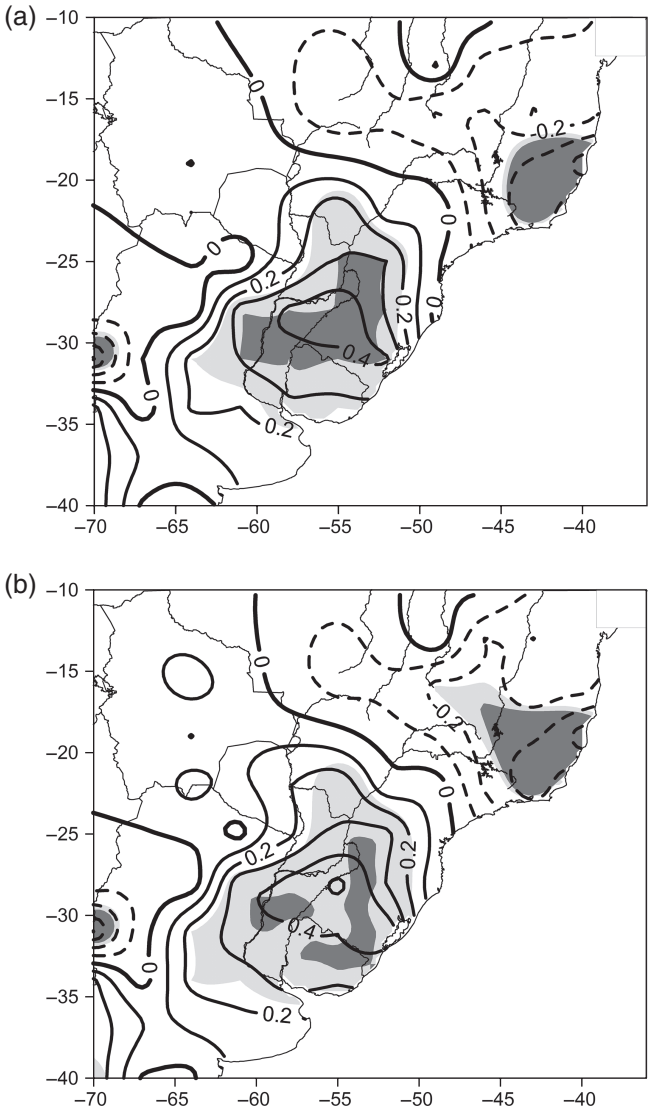

FIGURE 4 (a): Interannual correlation between factor loading 1 and precipitation. October–March, 1960–2012. Dark and light shadows indicate significant correlation at 95 and 90%. (b) Interannual correlation, but with detrended data, both in the factor loading and in precipitation series

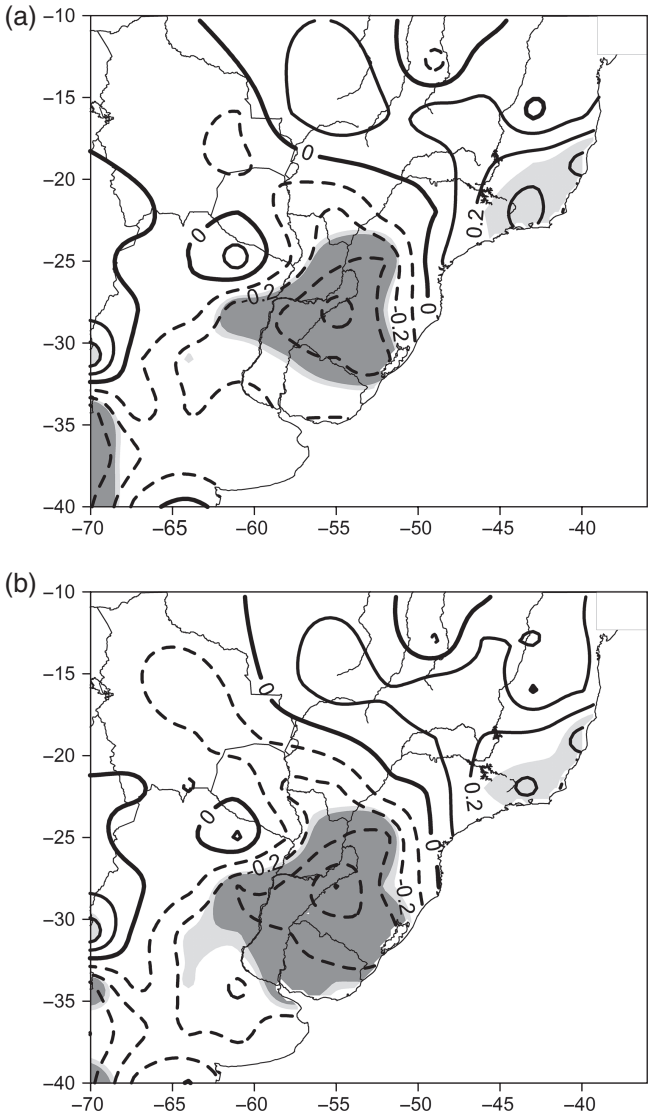

FIGURE 5 As in Figure 4, but for factor loading 2

represent adequately the precipitation field. Therefore, it makes sense to explore if part of this misrepresentation of the precipitation has to do with an inaccurate representation of the low level circulation variability. Figure 6 shows the two principal components of 18 GCMs, calculated over the same domain as in Figure 2 and for the same period, 1960–2012 of the warm season. The order of the two main modes of the Reanalysis is not always the same in the model PCA. For example, PC1 pattern in reanalysis is described by PC2 in models CCSM4, CSIRO-Mk3-6 and NorESM1-M, while PC1 of these models best matches the circulation of PC2 in the Reanalysis. The method for calculating PCs assigns their order according to the decreasing variance explained by each component. In the case of CCSM4 the variance explained by the two first components (Table 2) could be considered the same, hence any of these patterns could be considered the first principal component. In the case of the other two models the difference is not negligible, though still small. In this study we name PCs according to their variance and will use the term mode hence forth to group the two main patterns identified in the Reanalysis PCA.

In general, the two main modes in the models account for less variance percentage than in the observed case indicating that more variance is distributed in lower order modes. PC 1 and PC2 of 13 out of 19 models explain above 85% of the variance (Table 2) while the rest explain above 75%. This shows that the main two patterns resulting from the models PCA are similar to those resulting from the Reanalysis. These results are presented in Figure 6 as follows: Figure 6a groups those PC which resemble Reanalysis PC1 and which we will refer to henceforth as Mode 1, while Figure 6b depicts Mode 2 in the same manner.

From a visual inspection of the modes corresponding to the simulated fields by GCMs it can be concluded that they represent the main features of the observed interannual variability. In fact, all of them represent the northern flow over the south of SESA as well as a western flow at high latitudes

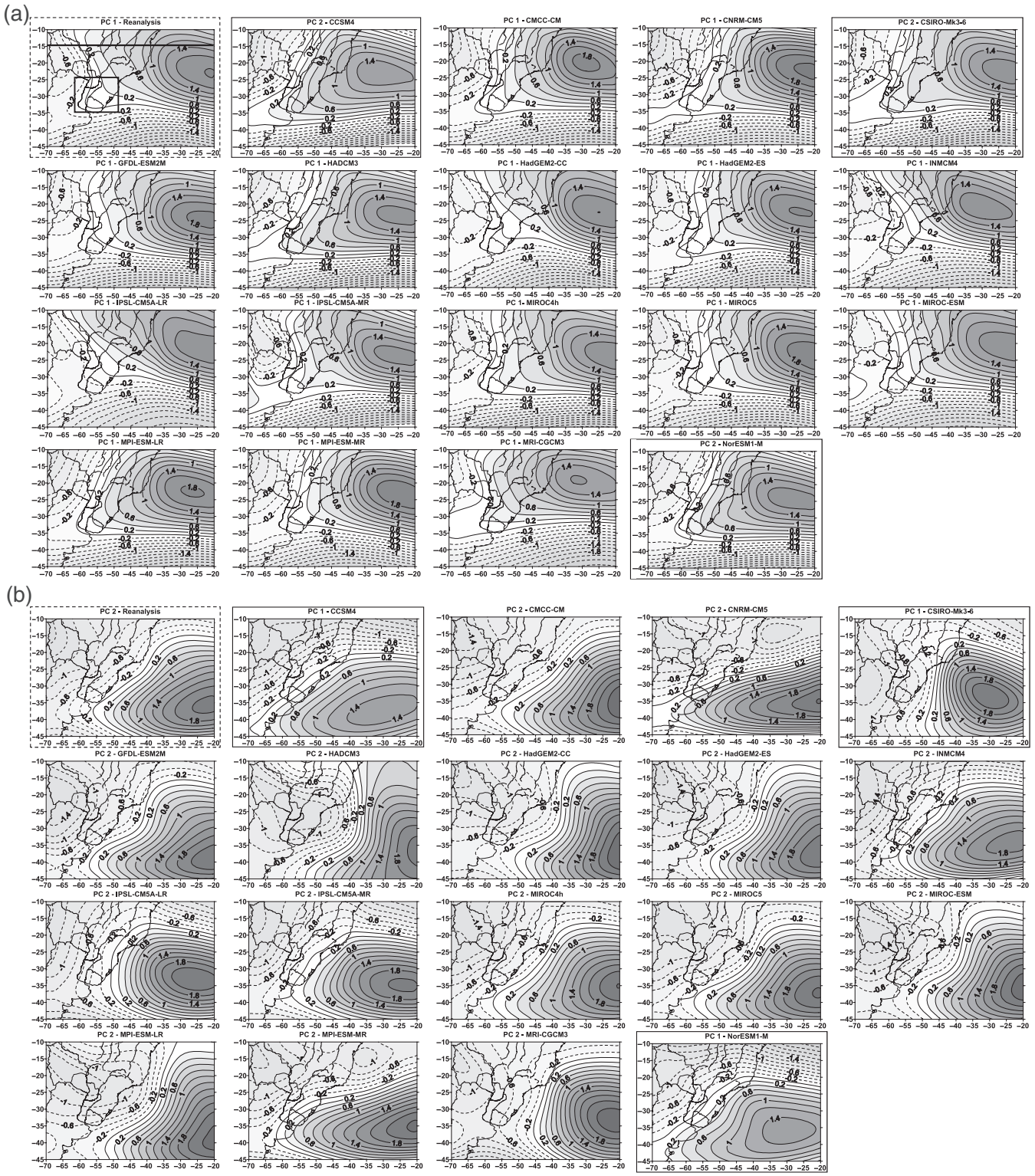

FIGURE 6 First two principal components of the interannual variability at low level circulation (streamflow at 925 hPa) of the warm season, 1960-2012 in 18 models as indicated in the figure. (a) Modes similar to the PC1 of the reanalysis and (b) those similar to PC2 of the reanalysis. Modes surrounded by a black box indicate models where the mode is represented by a different PC order than Reanalysis

in Mode 1 and the shift to the south of the south Atlantic High in Mode 2. This visual inspection however, also distinguishes differences between models and with the reanalysis. In Mode 1, the shape and intensity of the Atlantic Anticyclone presents differences, in 13 models the circulation enters the continent over Uruguay (box region in Figure 6a) while the clear exceptions are GFDL-ESM2M, HadGEM2-CC, INMCM4, MIROC-ESM where the westerlies dominate this region. The flow direction from equatorial latitudes over the continent towards SESA also presents differences at first sight. It varies from a marked northwestern flow in Reanalysis, HadGEM2-CC, INMCM4, IPSL-CM5A-

TABLE 2 Explained variance of GCMs first two modes and their accumulated value; correlation between observed modes 1 and 2 and the model PCs representing these modes

	Variance (%)			Correlation between model and observed modes	
GCM MODEL	**Mode 1**	**Mode 2**	**SUM**	**Mode 1**	**Mode 2**
CCSM4	44.6	44.7	89.3	0.90	0.86
CMCC-CM	48.7	35.0	83.7	0.98	0.98
CNRM-CM5	53.4	36.4	89.8	0.93	0.86
CSIRO-Mk3-6	42.8	44.9	87.7	0.98	0.89
GFDL-ESM2M	47.0	38.5	85.5	0.98	0.97
HadCM3	40.4	36.4	76.8	0.95	0.84
HadGEM2-CC	42.2	39.7	81.9	0.99	0.94
HadGEM2-ES	46.0	43.8	89.8	0.99	0.96
INMCM4	47.5	41.8	89.3	0.98	0.97
IPSL-CM5A-LR	45.9	42.8	88.7	0.97	0.92
IPSL-CM5A-MR	47.4	46.0	93.4	0.97	0.94
MIROC4h	49.5	46.9	96.4	0.99	0.98
MIROC5	47.6	46.5	94.1	0.99	0.98
MIROC-ESM	45.6	34.1	79.7	0.99	0.97
MPI-ESM-LR	46.4	30.3	76.7	0.96	0.91
MPI-ESM-MR	51.9	38.4	90.3	0.97	0.94
MRI-CGCM3	43.6	36.1	79.7	0.95	0.92
NorESM1-M	42.9	44.9	87.8	0.92	0.79
Average	46.08	40.62	86.7	0.97	0.92

LR, to a NNE flow in CCSM4, CNRM-CM5, HadCM3, MPI-ESM-LR and NorESM1-M, covering a variety of directions in between. Hence, this flow is not always from the Amazon region, in consequence the humid air advection towards SSESA may be reduced and lead to less precipitation. In the case of Mode 2, the changes in the shape, extension and position of the Atlantic Anticyclone are more evident. In CNRM-CM5 and MPI-ESM-MR a low pressure system over the ocean at 15°S restricts the position the anticyclone to higher latitudes. The position and intensity of the cyclonic circulation over the continent also is consistent with the position and shape of the anticyclone over the ocean. This is clear in the Hadley and MIROC models, GFDL and MPI-ESM-LR. The position of these two systems highly influences the circulation towards SESA and its convective and subsidence movements during the strong SACZ events, an indication of the misrepresentation of the SACZ dipole.

A method of evaluating the modes obtained by the models as compared to the Reanalysis is through Taylor diagrams (Taylor, 2001), where the fit of a model to observations is summarized graphically. Three parameters, correlation, their root-mean square difference and the amplitude of their variations are used to quantify the similarity between two patterns. Figure 7 presents the Taylor diagrams where statistics of the 18 models were computed for modes 1 (Figure 7a) and 2 (Figure 7b). Each model is assigned a coloured point and observations are identified by an empty circle. The position of each point appearing on the plot quantifies how closely the model's simulated results match the observations, in this case the

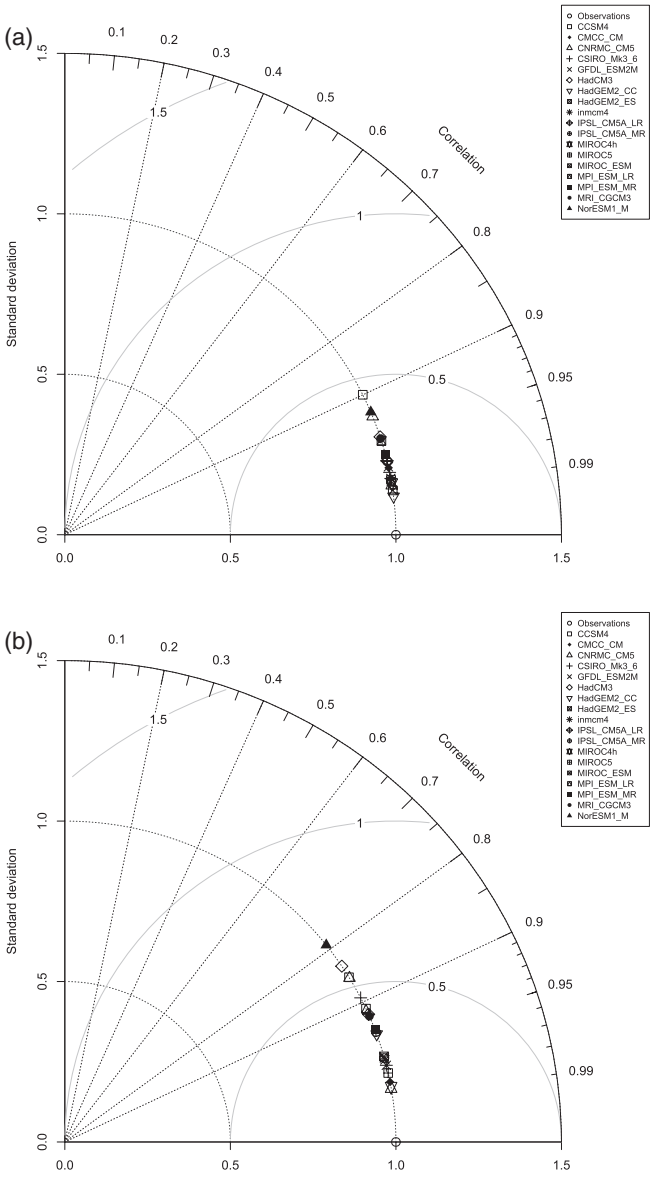

FIGURE 7 Taylor diagram for reanalysis and model: (a) Mode 1 and (b) Mode 2. The horizontal and vertical axes represent the *SD*s of the observation and model mode. The radial axis indicates the spatial correlation between the observation and model mode. The distance between the origin and any point is proportional to the RMSE

reanalysis modes. It can be seen that the pattern correlations are generally high (see also Table 2), above 0.9 in the case of Mode 1 with RMSE below 0.5 and mostly correlations above 0.8 in Mode 2 where the models with lowest correlation also present highest RMSE. The *SD* is 1 in all cases and modes on account of the standardization in the mathematical procedure used in PC analysis. According to this technique the models which best represents Mode 1 are HadGEM2-CC, HadGEM2-ES, MIROC4-h, MIROC-ESM, MIROC5 and the ones which may considered those that less adjust to the pattern are CCSM4 and NorESM1-M. The second mode of circulation is also best represented by the MIROC family of models together with CMCC-CM, GFDL-ESM2M and INMCM4 while NorESM1-M is the model which fails most in representing the circulation field.

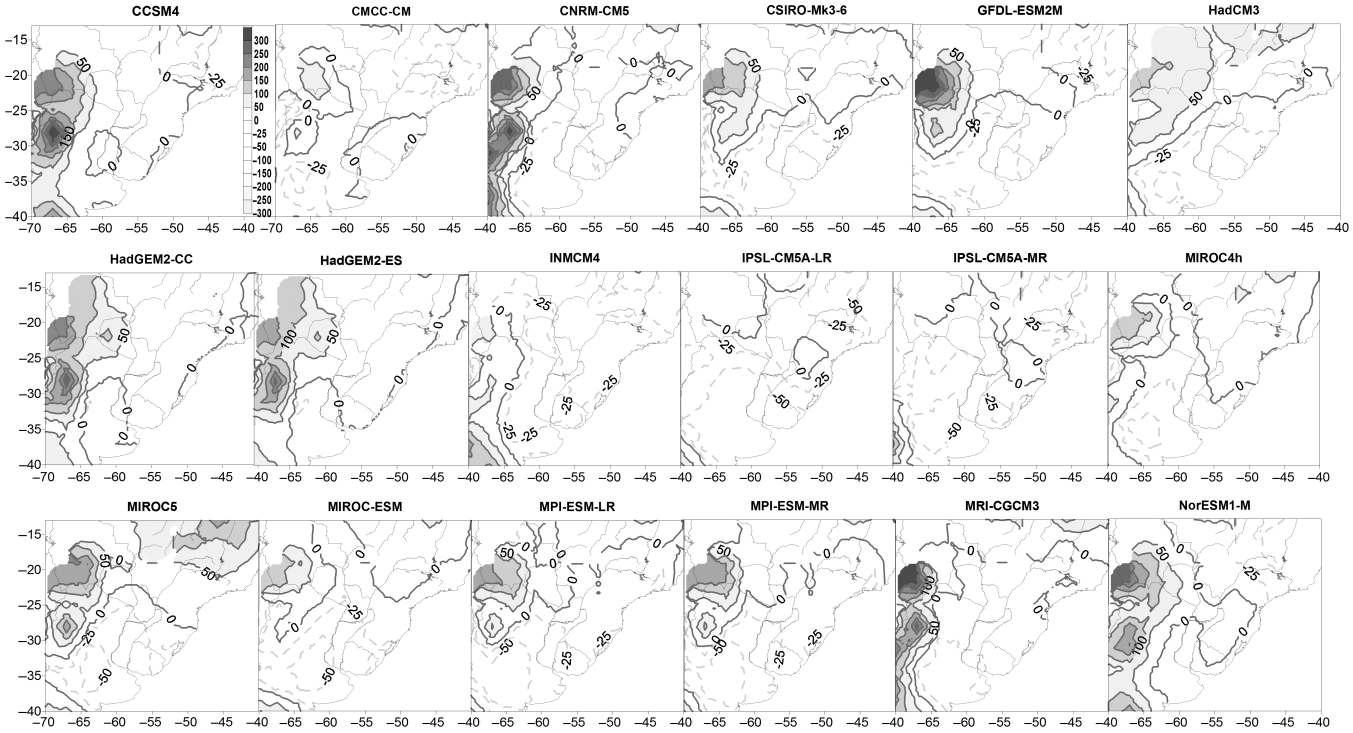

FIGURE 8 Precipitation relative error for 18 GCMs of the mean value with respect to observations

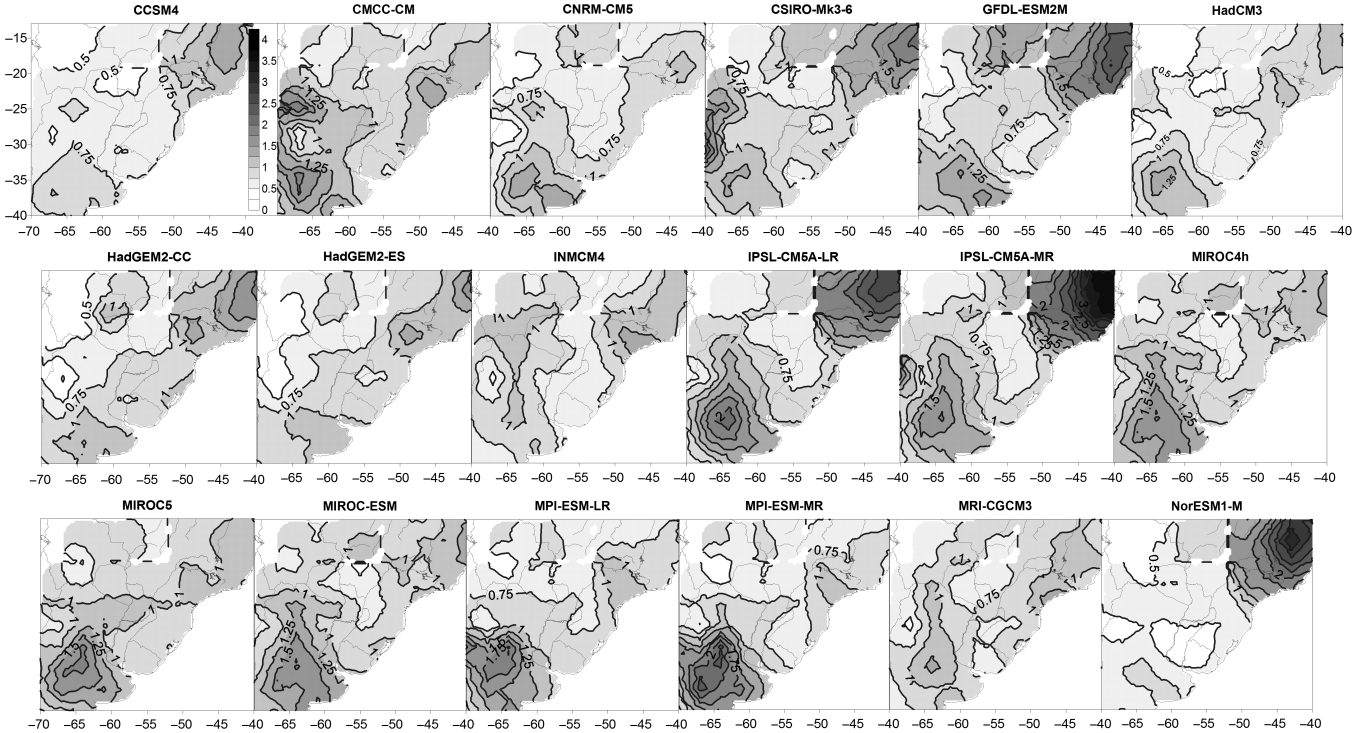

FIGURE 9 Precipitation coefficient of variation for 18 GCMs relative to the respective observed field period of 1960–2012

6 | GCMS MONTHLY VARIABILITY OF THE LOW LEVEL CIRCULATION AND MEAN PRECIPITATION

A relevant question that follows is how well each of the 18 GCMs represents the precipitation during the warm season. The relative error (Figure 8) and the interannual coefficient of variation (Figure 9) maps for each model show regions where models have problems in representing precipitation. Mean precipitation in the Andes region is overestimated by several models resulting in highly positive relative errors in the western longitudes in models such as CCSM4, CNRM-CM5, GFDL-ESM2M, HadGEM2-CC and ES, MIROC5, MPI-ESM-LR and MR, MRI-CGCM3 and NorESM1-M. Moving eastward, the pattern changes and mean precipitation is in general underestimated by the

GCMs, Figure 8, while the relative interannual variability is overestimated, with values above 1, particularly in south-eastern Brazil, Uruguay and central and eastern Argentina (Figure 9).

Figure 10 shows the Taylor diagram to assess the relative skill of the 18 GCMs in simulating the spatial pattern of the warm semester precipitation over the whole domain. The simulated patterns that agree well with observations lie nearest to the observations marked on the x-axis. This is the case of MIROC4h, MIROC-ESM and INMCM4, CMCC_CM models, which have high correlation and low RMSE.

Though MIROC4h has the highest correlation, it also presents higher spatial variability with respect to observations, the *SD* being 450 mm compared to the observed 350 mm. MIROC-ESM has a slightly higher correlation with observations than INMCM4 and it also presents a somewhat larger spatial variability, whereas INMCM4 *SD* is below the observed. Of the poorer performing models, NorESM1-M has a low pattern correlation, while MIROC5 has variations that are much larger than the observed; consequently both models have a large RMS error in the precipitation fields.

Table 3 ranks the adjustment to observations of the 18 GCMs according to the Taylor diagram, both for precipitation and for the two main low-level circulation modes; it also shows the Spearman's rank correlation coefficient (Zar, 2005) between their precipitation and circulation modes. The low values of the Spearman rank correlation. (0.05 and 0.22) indicates that not necessarily the best (worst) models representing the low-level circulation field are the best (worst) adjusting to the mean observed precipitation field. Precipitation is related to the low level circulation which provides the advection of water vapour, but it also depends on other dynamic and thermodynamic features that may not be well represented by the GCMs (Silva *et al.,* 2014). For example

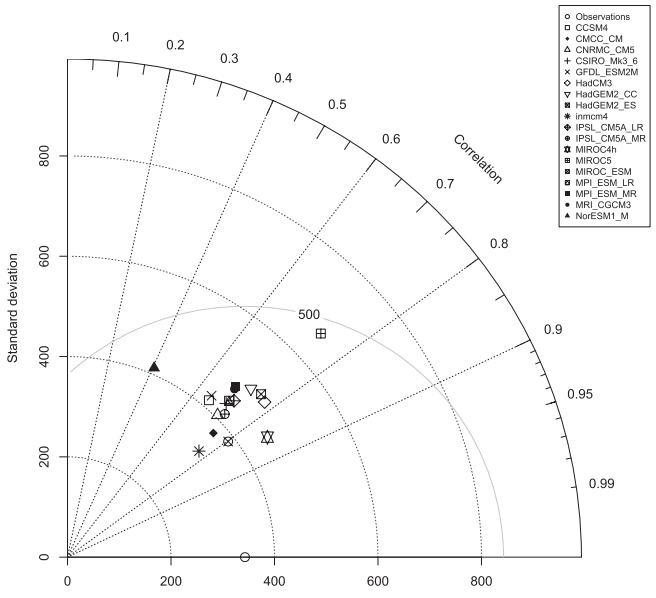

FIGURE 10 As Figure 7 but for precipitation

TABLE 3 Ranking of the MCGs according to their distance with observed values in the Taylor's diagrams (Figures 7a,b and 10)

MCG	Precipitation	CP1	CP2
MIROC_ESM	1	4	6
INMCM4	2	6	4
CMCC_CM	3	8	2
MIROC4h	4	3	1
CNRM_CM5	5	16	15
IPSL_CM5A_MR	6	11	12
CSIRO_Mk3_6	7	7	14
CCSM4	8	18	16
MPI_ESM_LR	9	13	10
MRI_CGCM3	10	14	11
GFDL_ESM2m	11	9	5
HadCM3	12	15	17
MPI_ESM_MR	13	12	13
IPSL_CM5A_LR	14	10	9
HadGEM2_ES	15	2	7
HadGEM2_CC	16	1	8
NorESM1_M	17	17	18
MIROC5	18	5	3
Spearman rank correlation between precipitation and CPs		0.05	0.22

Saurral *et al*. (2015) conclude that the altitude of the Andes Cordillera and the horizontal resolution in GCMs determine moisture fluxes and precipitation over regions of South America, such as SESA.

The region inside the square, east of 61°W and west of 48°W between 25° and 35°S, first panel of Figure 6, from now on the box region, deserves additional attention, not only because it has a clear signal of a relationship between the low-level circulation modes, Figures 4 and 5, but also because it is one of more developed and populated areas of South America. Therefore it is important to understand what features of the GCMs are necessary to improve future climate scenarios. In spite of the significant correlation between the main low-level circulation modes and mean precipitation in SSESA (Figures 4 and 5), most GCMs underestimate this precipitation (Table 4) with the exception of HadGEM2-CC and ES, and CCSM4, and in general present higher coefficient of variation than the observed, except CCSM4 and NorESM1-M with a coefficient of variation equal to and below 1, respectively. The average underestimation of mean precipitation across models was 16%. In addition, more than half of them underestimate the warm season precipitation by more than 20%, Table 4. This error level compromises the use of these models to assess future precipitation because most GCMs, with different greenhouse gas concentrations for either near future or for the end of the century, project future precipitation changes, close to or less than 20% of the recent average precipitation in this region (Jones and Carvalho, 2013; Chou *et al.,* 2014; Lee and Wang, 2014).

TABLE 4 Precipitation error and coefficient of variation in the box region and fluxes from the north towards this region

GCM MODEL	Precipitation relative error in the box region (%)	Interannual precipitation coefficient of variation in the box region	INDEX flux at 15° directed towards the box region
Reanalysis		1	0.8
CCSM4	3.4	1	0.7
CMCC-CM	−2.5	1.1	0.8
CNRM-CM5	−19.0	1.5	0.6
CSIRO-Mk3–6	−23.0	1.4	0.5
GFDL-ESM2M	−24.0	1.3	0.5
HadCM3	−24.0	1.2	0.3
HadGEM2-CC	6.0	1.1	0.3
HadGEM2-ES	6.0	1.2	0.6
INMCM4	−26.0	1.1	0.3
IPSL-CM5A-LR	−38.0	2.1	0.1
IPSL-CM5A-MR	−23.0	1.6	0.6
MIROC4h	−9.0	1.3	0.7
MIROC5	−20.0	1.6	0.6
MIROC-ESM	−28.0	1.2	0.5
MPI-ESM-LR	−23.0	1.3	0.5
MPI-ESM-MR	−23.0	1.2	0.6
MRI-CGCM3	−16.0	1.1	0.5
NorESM1-M	−1.0	0.92	0.6
Average	−15.8	1.22	0.5

Water vapour sources for southeastern South America rainfall only comes either from the tropical humid continent or from the Atlantic Ocean (Labraga *et al.,* 2002; Barros *et al.,* 2003; Saurral *et al.,* 2015). Moist air from the Pacific Ocean cannot reach this region because of the Andes barrier that from 40°S to the north is higher than the 700 hPa level. Thus the following discussion focuses only on the flows from the north and the Atlantic Ocean.

Although, the spatial patterns of the first two modes are in general well represented by all models, Table 2, there are key features that deserve further analysis. In the case of Mode 1, one of these features is the flow which advects warm and humid air into SSESA from the tropical humid continent. The flow into the box region depicted by Mode 2 also brings moist air, in this case from the coastal areas of the Atlantic Ocean, but it has an anticyclonic circulation that averts rainfall; thus this flow is not expected to be related with rainfall over the box region. Therefore, only the first mode of the low level circulation was used to represent the intensity of the northern flow from the tropical continent in the box region. Since this flow is proportional to the zonal stream function PC gradient, the difference between the two longitude extremes of the square box at 25°S can stand for this gradient and it is used here as a proxy index for the northern flow entering the box region. For example the northern flow index (NFI) of the reanalysis is 0.8 resulting from the difference of the stream function PC1 at the two extremes of the square box at 25°S, Figure 6a, first panel.

In the reanalysis and in all GCMs the northern flow so calculated crosses 15°S from the tropical continent, Figure 6a. Hence the NFI stands from the flow coming only from the tropical continent. The value of the NFI for each model is presented in the last column of Table 4.

All models except CCSM4 have a NFI below 0.8, the reanalysis reference value, Table 4, indicating that the flow from the tropical continent into SSESA is underestimated by most models. In addition, correlation across the 18 models between their relative precipitation error and the mentioned NFI is 0.5, significant at 95% level. Figure 11 depicts graphically values shown in Table 4 and helps to visualize the dependence of precipitation error on the northern flow from the tropical continent in the GCMs. This result indicates that misrepresentation of the northern humid and warm flow from the tropical continent is a cause of the underestimation of precipitation in the SSESA region by GCMs.

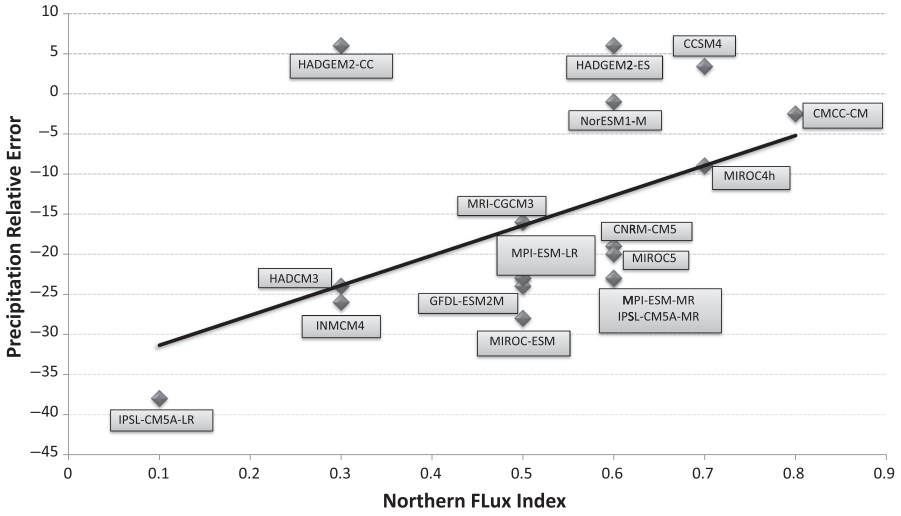

FIGURE 11 GCMs precipitation relative error in the SSESA region as a function of their northern flux index into it as explained in the text

7 | CONCLUDING REMARKS

The analysis of 18 CMIP5 GCM simulations from 1960 to 2012 indicates that models represent well the large features of the low level circulation variability of the warm season (October to March) over SSESA (southeastern Brazil, Uruguay and central and eastern Argentina) and particularly the relevant regional feature of the switch between the two flow patterns associated with the active and weak SACZ, Figure 6.

However, the best (worst) models in representing the low circulation modes, not necessarily are the best (worst) in doing so with the mean precipitation over the whole domain that includes South East South America, east of the Andes, Table 3.

In the case of the SSESA, interannual warm season precipitation was correlated during 1960–2012 with the two main modes of the two low level circulation that represent the flow from the tropical continent to either this region or to the SACZ, Figures 3 and 4. However, spite of the good representation of these modes by the GCMs, most of them underestimate the mean warm season precipitation and overestimate the interannual variability in SSESA, Figures 8 and 9.

A closer look at the low level circulation modes of the GCMs showed that the northern flow, which carries hot and humid air to SSESA, was underestimated by most of the models, Table 4. The significant correlation (0.5) found across GCMs between the mean precipitation and a low level northern flow index over this region indicates that underestimation of this northern flow is one cause for the precipitation deficit. Of course, they may be other sources of error, like a not well fitted cloud and precipitation parameterizations or other misrepresented circulation features. The models with best Northern flow index were CMCC-CM, CCSM4 and MIROC-4h; the first two were also second and third in the rank of adjustment to the mean precipitation over SSESA.

ACKNOWLEDGEMENTS

This work was supported by CONICET under the grant PIP 11220120100586 and by UBACYT grant 20020130100644BA.

ORCID

Moira E. Doyle https://orcid.org/0000-0003-0858-8999

REFERENCES

Barros, V., Doyle, M., González, M., Camilloni, I., Bejarán, R. and Caffera, R. (2003) Climate variability over subtropical South America and the South American Monsoon: a review. *Meteorologica*, 27, 34–58.

Barros, V., Doyle, M. and Camilloni, I. (2008) Precipitation trends in southeastern South America: relationship with ENSO phases and with low-level circulation. *Theoretical and Applied Climatology*, 93, 19–33. https://doi.org/10.1007/s00704-007-0329-x.

Biasutti, M., Sobel, A. and Kushnir, Y. (2006) AGCM precipitation biases in the Tropical Atlantic. *Journal of Climate*, 19, 935–957. https://doi.org/10.1175/JCLI3673.1.

Blazquez, J. and Nuñez, M. (2013) Analysis of uncertainties in future climate projections for South America: comparison of WCRP-CMIP3 and WCRP-CMIP5 models. *Climate Dynamics*, 41, 1039–1056. https://doi.org/10.1007/s00382-012-1489-7.

Boers, N., Rheinwalt, A., Bookhagen, B., Barbosa, H.M.J., Marwan, N., Marengo, J. and Kurths, J. (2014) The South American rainfall dipole: a complex network analysis of extreme events. *Geophysical Research Letters*, 41, 7397–7405. https://doi.org/10.1002/2014GL061829.

Bombardi, R.J. and Carvalho, L.M.V. (2011) The South Atlantic dipole and variations in the characteristics of the South American Monsoon in the WCRP-CMIP3 multi-model simulations. *Climate Dynamics*, 36, 2091–2102. https://doi.org/10.1007/s00382-010-0836-9.

Boulanger, J.-P., Martinez, F. and Segura, E.C. (2007) Projection of future climate change conditions using IPCC simulations, neural net- works and Bayesian statistics. Part 2: precipitation mean state and seasonal cycle in South America. *Climate Dynamics*, 28, 255–271. https://doi.org/10.1007/s00382-006-0182-0.

Brown, J.R., Moise, A.F. and Colman, R.A. (2013) The South Pacific Convergence Zone in CMIP5 simulations of historical and future climate. *Climate Dynamics*, 41, 2179–2197. https://doi.org/10.1007/s00382-012-1591-x.

Camilloni, I., Doyle, M. and Barros, V. (2004) *Interannual Variability of the South Atlantic High and Rainfall in Southeastern South America During Summer Months*. Fortaleza, Brazil: XIII Congresso Brasileiro de Meteorologia.

Carvalho, L.M.V., Jones, C. and Liebmann, B. (2004) The South Atlantic Convergence Zone: intensity, form, persistence, and relationships with intraseasonal to interanual activity and extreme rainfall. *Journal of Climate*, 17, 88–108.

Catto, J.L., Shaffrey, L.C. and Hodges, K.I. (2010) Can climate models capture the structure of extratropical cyclones? *Journal of Climate*, 23, 1621–1635.

Catto, J.L., Jakob, C., Berry, G. and Nicholls, N. (2012) Relating global precipitation to atmospheric fronts. *Geophysical Research Letters*, 39, L10805. https://doi.org/10.1029/2012GL051736.

Catto, J.L., Jakob, C. and Nicholls, N. (2013) A global evaluation of fronts and precipitation in the ACCESS model. *Australian Meteorological Oceanographic Society Journal*, 63, 191–203.

Chou, S.C., Lyra, A., Mourao, C., Dereczynski, C., Pilotto, I., Gomes, J., Bustamente, J., Tavares, P., Silva, A., Rodrigues, D., Campos, D., Chagas, D., Sueiro, G., Siqueira, G. and Marengo, J. (2014) Assessment of Climate Change over South America under RCP 4.5 and 8.5 Downscaling Scenarios. *American Journal of Climate Change*, 3, 512–527. https://doi.org/10.4236/ajcc.2014.35043.

Cressie, N.A.C. (1991) *Statistics for Spatial Data*. New York: John Wiley and Sons, p. 900.

Da Silva, A. (2007). GrADS Extension Library for Calculating Streamfunction/Velocity Potential. Availabel at: http://opengrads.org/doc/udxt/fish/fish.html

Dai, A. (2006) Precipitation characteristics in eighteen coupled climate models. *Journal of Climate*, 19, 4605–4630. https://doi.org/10.1175/JCLI3884.1.

Davey, M., Huddleston, M., Sperber, K., et al. (2002) STOIC: a study of coupled model climatology and variability in the tropical ocean regions. *Climate Dynamics*, 18, 403–420. https://doi.org/10.1007/s00382-001-0188-6.

Delworth, T.L., Rosati, A., Anderson, W., Adcroft, A.J., Balaji, V., Benson, R., Dixon, K., Griffies, S.M., Lee, H., Pacanowski, R.C., Vecchi, G.A., Wittenberg, A.T., Zeng, F. and Zhang, R. (2012) Simulated climate and climate change in the GFDL CM2.5 high-resolution coupled climate model. *Journal of Climate*, 25, 2755–2781. https://doi.org/10.1175/JCLI-D-11-00316.1.

Demory, M.E., Vidale, P.L., Roberts, M.J., Berrisford, P., Strachan, J., Schiemann, R. and Mizielinski, M.S. (2014) The role of horizontal resolution in simulating drivers of the global hydrological cycle. *Climate Dynamics.*, 42, 2201–2225. https://doi.org/10.1007/s00382-013-1924-4.

Doyle, M.E. and Barros, V.R. (2002) Midsummer low-level circulation and precipitation in subtropical South America and related sea surface temperature anomalies in the South Atlantic. *Journal of Climate*, 15, 3394–3410. https://doi.org/10.1175/1520-0442(2002)015<3394:MLLCAP>2.0.CO;2.

Flato, G., Marotzke, J., Abiodun, B., Braconnot, P., Chou, S.C., Collins, W., Cox, P., Driouech, F., Emori, S., Eyring, V., Forest, C., Gleckler, P., Guilyardi, E., Jakob, C., Kattsov, V., Reason, C. and Rummukainen, M. (2013) Evaluation of climate models. In: Stocker, T.F. , Qin, D. , Plattner, G.-K. , Tignor, M. , Allen, S.K. , Boschung, J. , Nauels, A. , Xia, Y. , Bex, V. and Midgley, P.M. (Eds.) *Climate Change 2013: The Physical Science Basis. Contribution of Working Group I to the Fifth Assessment Report of the Intergovernmental Panel on Climate Change*. Cambridge, UK and New York, NY: Cambridge University Press.

Gandú, A.W. and Silva Días, P.L. (1998) Impact of tropical heat sources on the South American tropospheric circulation and subsidence. *Journal of Geophysical Research*, 103, 6001–6015. https://doi.org/10.1029/97JD03114.

Geil, K.L., Serra, Y.L. and Zeng, X. (2013) Assessment of CMIP5 model simulations of the north American monsoon system. *Journal of Climate*, 26, 8787–8801. https://doi.org/10.1175/JCLI-D-13-00044.1.

Grimm, A.M., Barros, V.R. and Doyle, M.E. (2000) Climate variability in southern South America associated with El Niño and La Niña Events. *Journal of Climate*, 13, 35–58. https://doi.org/10.1175/1520-0442(2000)013<0035:CVISSA>2.0.CO;2.

Gulizia, C. and Camilloni, I. (2015) Comparative analysis of the ability of a set of CMIP3 and CMIP5 global climate models to represent precipitation in South America. *International Journal of Climatology*, 35, 583–595. https://doi.org/10.1002/joc.4005.

Gulizia, C., Camilloni, I. and Doyle, M. (2013) Identification of the principal patterns of summer moisture transport in South America and their representation by WCRP/CMIP3 global climate models. *Theoretical and Applied Climatology.*, 112, 227–241. https://doi.org/10.1007/s00704-012-0729-4.

Hu, Y. and Fu, Q. (2007) Observed poleward expansion of the Hadley circulation since 1979. *Atmospheric Chemistry and Physics*, 7, 5229–5236.

IPCC. (2007) *Climate Change. The Scientific Basis*. Geneva, Switzerland: Cambridge University Press.

IPCC. (2013) Climate change 2013: the physical science basis. In: Stocker, T.F. , Qin, D. , Plattner, G.-K. , Tignor, M. , Allen, S.K. , Boschung, J. , Nauels, A. , Xia, Y. , Bex, V. and Midgley, P.M. (Eds.) *Contribution of Working Group I to the Fifth Assessment Report of the Intergovernmental Panel on Climate Change*. Cambridge, UK and New York, NY: Cambridge University Press, p. 1535.

Jones, C. and Carvalho, L. (2013) Climate change in the south American monsoon system: present climate and CMIP5 projections. *Journal of Climate*, 26, 6660–6678. https://doi.org/10.1175/JCLI-D-12-00532.1.

Kalnay, E., Kanamitsu, M., Kistler, R., Collins, W., Deaven, D., Gandin, L., Iredell, M., Sha, S., White, G., Woollen, J., Zhu, Y., Chelliah, M., Ebisuzaki, W., Higgins, W., Janowiak, J., Mo, K.C., Ropelewski, C., Wang, J., Leetmaa, A., Reynolds, R., Jenne, R. and Joseph, D. (1996) The NCEP/NCAR 40-year reanalysis project. *Bulletin of the American Meteorological Society*, 77, 437–471. https://doi.org/10.1175/1520-0477(1996)077<0437:TNYRP>2.0.CO;2.

Kantelhardt, J.W., Koscielny-Bunde, E., Rego, H.H.A., Havlin, S. and Bunde, A. (2001) Detecting long-range correlations with detrended fluctuation analysis. *Physica A*, 295, 441–454. https://doi.org/10.1016/S0378-4371(01)00144-3.

Kistler, R., et al. (2001) The NCEP–NCAR 50-year reanalysis: monthly means CD-ROM and documentation. *Bulletin of the American Meteorological Society*, 82, 247–267. https://doi.org/10.1175/1520-0477(2001)082<0247:TNNYRM>2.3.CO;2.

Labraga, J.C., Scian, B. and Frumento, O. (2002) Anomalies in the atmospheric circulation associated with the rainfall excess or déficit in the Pampa Region in Argentina. *Journal of Geophysical Research*, 107(D23), 4666–ACL 2-15. https://doi.org/10.1029/2002JD002113.

Lawrimore, J.H., Menne, M.J., Gleason, B.E., Williams, C.N., Wuertz, D.B., Vose, R.S. and Rennie, J. (2011) An overview of the global historical climatology network monthly mean temperature data set, version 3. *Journal of Geophysical Research*, 116, D19121. https://doi.org/10.1029/2011JD016187.

Lee, J.-Y. and Wang, B. (2014) Future change of global monsoon in the CMIP5. *Climate Dynamics*, 42, 101–119. https://doi.org/10.1007/s00382-012-1564-0.

Levang, S.J. and Schmitt, R.W. (2015) Centennial changes of the global water cycle in CMIP5 models. *Journal of Climate*, 28, 6489–6502. https://doi.org/10.1175/JCLI-D-15-0143.1.

Liebmann, B., Vera, C.S., Carvalho, L.M.V., Camilloni, I.A., Hoerling, M.P., Allured, D., Barros, V.R., Baez, J. and Bidegain, M. (2004) An observed trend in central south American precipitation. *Journal of Climate*, 17, 4357–4367.

Marengo, J.A., Liebmann, B., Grimm, A.M., Misra, V., Silva Dias, P.L., Cavalcanti, I.F.A., Carvalho, L.M.V., Berbery, E.H., Ambrizzi, T., Vera, C.S., Saulo, A.C., Nogues-Paegle, J., Zipser, E., Seth, A. and Alves, L.M. (2012) Recent developments on the south American monsoon system. *International Journal of Climatology*, 32, 1–21. https://doi.org/10.1002/joc.2254.

Mehran, A., AghaKouchak, A. and Phillips, T.J. (2014) Evaluation of CMIP5 continental precipitation simulations relative to satellite-based gauge-adjusted observations. *Journal of Geophysical Research Atmospheres*, 119, 1695–1707. https://doi.org/10.1002/2013JD021152.

Mo, K.C. and Berbery, E.H. (2011) Drought and persistent wet spells over South America based on observations and the U.S. CLIVAR drought experiments. *Journal of Climate*, 24, 1801–1820. https://doi.org/10.1175/2010JCLI3874.1.

Neale, R.B., Richter, J.H. and Jochum, M. (2008) The impact of convection on ENSO: from a delayed oscillator to a series of events. *Journal of Climate*, 21, 5904–5924.

Nogués-Paegle, J. and Mo, K.C. (1997) Alternating wet and dry conditions over South America during summer. *Monthly Weather Review*, 125, 279–291. https://doi.org/10.1175/1520-0493(1997)125<0279:AWADCO>2.0.CO;2.

Penalba, O. and Vargas, W.M. (2008) Variability of low monthly rainfall in La Plata Basin. *Meteorological Applications*, 15, 313–323. https://doi.org/10.1002/met.68.

Pfahl, S. and Wernli, H. (2012) Quantifying the relevance of cyclones for precipitation extremes. *Journal of Climate*, 25, 6770–6780. https://doi.org/10.1175/JCLI-D-11-00705.1.

Polvani, L.M., Waugh, D.W., Correa, G.J.P. and Son, S.-W. (2011) Stratospheric ozone depletion: the main driver of twentieth-century atmospheric circulation changes in the southern hemisphere. *Journal of Climate*, 24, 795–811. https://doi.org/10.1175/2010JCLI3772.1.

Rencher, A.C. (1998) *Multivariate Statistical Inference and Applications*. New York, NY: John Wiley and Sons Inc., p. 559.

Richman, M.B. (1986) Rotation of principal components: a review. *International Journal of Climatology*, 6, 293–336. https://doi.org/10.1002/joc.3370060305.

Richter, I. and Xie, S.P. (2010) Moisture transport from the Atlantic to the Pacific basin and its response to North Atlantic cooling and global warming. *Climate Dynamics*, 35, 551–566. https://doi.org/10.1007/s00382-009-0708-3.

Sakaguchi, K., Zeng, X. and Brunke, M.A. (2012) Temporal- and spatial-scale dependence of three CMIP3 climate models in simulating the surface temperature trend in the twentieth century. *Journal of Climate*, 25, 2456–2470. https://doi.org/10.1175/JCLI-D-11-00106.1.

Saurral, R.I., Camilloni, I.A. and Ambrizzi, T. (2015) Links between topography, moisture fluxes pathways and precipitation over South America. *Climate Dynamics.*, 45, 777–789. https://doi.org/10.1007/s00382-014-2309-z.

Schmittner, A., Silva, T.A.M., Fraedrich, K., Kirk, E. and Lunkeit, F. (2011) Effects of mountains and ice sheets on global ocean circulation. *Journal of Climate*, 24, 2814–2829. https://doi.org/10.1175/2010JCLI3982.1.

Seager, R., Naik, N., Baethgen, W., Robertson, A., Kushnir, Y., Nakamura, J. and Jurburg, S. (2010) Tropical oceanic causes of interannual to multidecadal precipitation variability in Southeast South America over the past century. *Journal of Climate*, 23, 5517–5539. https://doi.org/10.1175/2010JCLI3578.1.

Sillmann, J., Kharin, V.V., Zhang, X. and Zwiers, F.W. (2013) Climate extreme indices in the CMIP5 multi-model ensemble. Part 1: model evaluation in the present climate. *Journal of Geophysical Research*, 118(4), 1716–1733. https://doi.org/10.1002/jgrd.50203.

Silva, G.A., Dutra, L.M., daRocha, R.P., Ambrizzi, T. and Leiva, É. (2014) Preliminary analysis on the global features of the NCEP CFSv2 seasonal hindcasts. *Advances in Meteorology*, 2014, 695067. https://doi.org/10.1155/2014/695067.

Silvestri, G. and Vera, C. (2008) Evaluation of the WCRP-CMIP3 model simulations in the La Plata Basin. *Meteorological Applications*, 15, 497–502. https://doi.org/10.1002/met.98.

Solman, S.A., Nuñez, M.N. and Cabre, M.F. (2008) Regional climate change experiments over southern South America. I: present climate. *Climate Dynamics*, 30, 533–552. https://doi.org/10.1007/s00382-007-0304-3.

Stephens, G.L., L'Ecuyer, T., Forbes, R., Gettlemen, A., Golaz, J.-C., Bodas-Salcedo, A., Suzuki, K., Gabriel, P. and Haynes, J. (2010) Dreary

state of precipitation in global models. *Journal of Geophysical Research*, 115, D24211. https://doi.org/10.1029/2010JD014532.

Stockdale, T., Balmaseda, M. and Vidard, A. (2006) Tropical Atlantic SST prediction with coupled ocean–atmosphere GCMs. *Journal of Climate*, 19, 6047–6061. https://doi.org/10.1175/JCLI3947.1.

Sun, Y., Solomon, S., Dai, A. and Portmann, R.W. (2007) How often will it rain? *Journal of Climate*, 20, 4801–4818. https://doi.org/10.1175/JCLI4263.1.

Taylor, K.E. (2001) Summarizing multiple aspects of model performance in a single diagram. *Journal of Geophysical Research*, 106(D7), 7183–7192. https://doi.org/10.1029/2000jd900719.

Taylor, K.E., Stouffer, R.J. and Meehl, G.A. (2012) An overview of CMIP5 and the experiment design. *Bulletin of the American Meteorological Society*, 93, 485–498. https://doi.org/10.1175/BAMS-D-11-00094.1.

Tian, B., Fetzer, E.J., Kahn, B.H., Teixeira, J., Manning, E. and Hearty, T. (2013) Evaluating CMIP5 models using AIRS tropospheric air temperature and specific humidity climatology. *Journal of Geophysical Research Atmospheres.*, 118, 114–134. https://doi.org/10.1029/2012JD018607.

Vera, C., Silvestri, G., Liebmann, B. and González, P. (2006a) Climate change scenarios for seasonal precipitation in South America from IPCC-AR4 models. *Geophysical Research Letters*, 33, L13707. https://doi.org/10.1029/2006GL025759.

Vera, C., Higgins, W., Amador, J., Ambrizzi, T., Garreaud, R., Gochis, D., Gutzler, D., Lettenmaier, D., Marengo, J., Mechoso, C., Nogues-Paegle, J., Silva Dias, P. and Zhang, C. (2006b) Toward a unified view of the American monsoon systems. *Journal of Climate*, 19, 4977–5000. https://doi.org/10.1175/JCLI3896.1.

Yin, L., Fu, R., Shevliakova, E. and Dickson, R. (2013) How well can CMIP5 simulate precipitation and its controlling processes over tropical South America? *Climate Dynamics*, 41, 3127–3143. https://doi.org/10.1007/s00382-012-1582-y.

Yongyun, H., Ch, Z. and Jiping, L. (2011) Observational evidence for poleward expansion of the Hadley circulation. Advances y circulation. *Advances in Atmospheric Sciences*, 28, 33–44. https://doi.org/10.1007/s00376-010-0032-1.

Zar, J.H. (2005) Spearman rank correlation. In: Armitage, P. and Colton, T. (Eds.) *Encylopedia for Biostatistics*. https://doi.org/10.1002/0470011815.b2a15150.

Zhou, J. and Lau, K.M. (1998) Does a monsoon climate exist over South America? *Journal of Climate*, 11, 1020–1040.

How to cite this article: Barros VR, Doyle ME. Low-level circulation and precipitation simulated by CMIP5 GCMS over southeastern South America. *Int J Climatol*. 2018;38:5476–5490. https://doi.org/10.1002/joc.5740